Novel calibration optical path of cryogenic radiometer

Weiwei Pang (庞伟伟)[1], Xiaobing Zheng (郑小兵)[1], Jianjun Li (李健军)[1],*,
Xueshun Shi (史学舜)[2], Haoyu Wu (吴浩宇)[1], Maopeng Xia (夏茂鹏)[1],
Dongyang Gao (高冬阳)[1], Jianmin Shi (史剑民)[1], Tao Qi (戚涛)[1], and Qing Kang (康晴)[1]

[1]*Key Laboratory of Optical Calibration and Characterization, Chinese Academy of Sciences, Hefei 230031, China*
[2]*The 41st Institute of China Electronics Technology Group Corporation, Qindao 266555, China*
*Corresponding author: jjli@aiofm.ac.cn

We introduce a novel calibration optical path of the cryogenic radiometer, which can avoid the repeated dismounting measurement and eliminate the negative influence of Brewster window effect on calibration result. The novel calibration optical path is used to calibrate the absolute spectral responsivity of the standard transfer detector at 633 nm, the results of which are compared with the ones of the previous structure. It is shown that comparing the previous results to the structure optimization, the measurement uncertainty of laser power reduces by a factor of 2, the measurement uncertainty on the absolute spectral responsivity of the transfer detector decreases by 15%, and the consistence of the calibration on absolute spectral responsivity is 4.0×10^{-3}. The experiment result proves that the novel calibration optical path of cryogenic radiometer can effectively reduce the calibration uncertainty against standard detector and improve the accuracy of calibration.

OCIS codes: 120.3930, 120.3940, 120.4570, 120.4640, 120.4800.
doi: 10.3788/COL201513.051201.

The application of cryogenic radiometer is a breakthrough in the measuring region of optical radiation with high precision. The measurement of laser power by means of cryogenic radiometer reaches a very high precision due to the fact that it combines electrical substitution, low temperature, and superconductivity technology. The significant achievement especially lies in the uncertainty of 0.005%–0.02% for the measurement of visible bands[1–3]. Figure 1 shows the principle based on the cryogenic radiometer to measure laser power. The stably adjusted incident laser would lose its congenital power when penetrating Brewster window before entering the reception cavity of the cryogenic radiometer. The laser radiation measurement through cryogenic radiometer is based on the equivalence principle of electrical heating and light-radiation heating which would dismount Brewster window of cryogenic radiometer and reproduce the state when the window measures the laser power as well as measure the transmittance of the window and the internal loss[4,5]. At last, it calculates the power of incident laser after comprehensively taking the previous measurement process into consideration. The equation of state can be showed as

$$P_L = \frac{1}{T}\left(\frac{NP_h}{A} + P_S\right), \tag{1}$$

where P_L is the power of incident laser which is to be measured, T represents the window transmittance of cryogenic radiometer, A is the absorptivity of the reception cavity, N stands for the equivalence factor of electrical heating and light-radiation heating, P_h is the power of electrical heating, i.e., direct output value of cryogenic

radiometer, and P_s is the loss power caused by the surface reflection and internal scattering of the window.

Limited to the influence from the structure and operation condition, generally speaking, cryogenic radiometer is used as the primary standard of radiation in the laboratory[6–9] while it is not directly used as the work standard to calibrate the application instruments. In order to establish standard transfer chain of radiation which is based on cryogenic radiometer, it is necessary to develop the standard detector which is with high precision in spectral responsivity in different wavelengths. Through using the cryogenic radiometer to calibrate the absolute spectral responsivity of transfer detector, the detector then could be used as work standard to calibrate the application instruments[10–12].

Figure 2 shows the calibration principle for the transfer detector by means of cryogenic radiometer. In front of the Brewster window a linear guide which was perpendicular
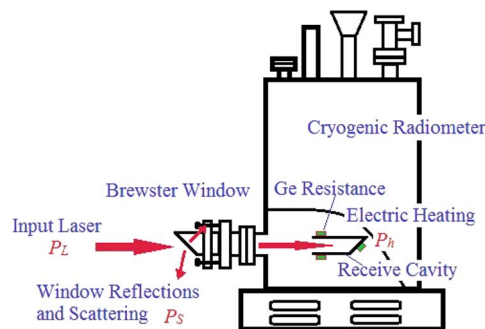

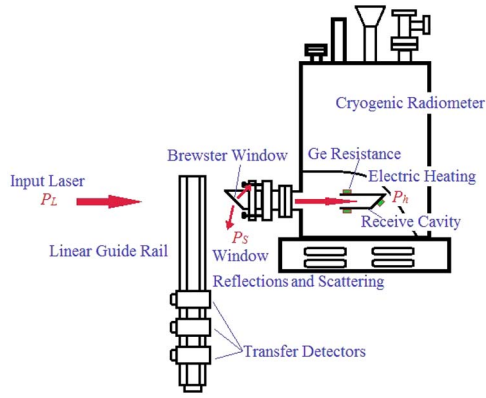Fig. 1. Laser power measurement based on cryogenic radiometer.

Fig. 2. Transfer detector on calibration of cryogenic radiometer.

to the optical path was assembled. The transfer detector was installed on the guide rail. The incident beam P_L successively entered the cryogenic radiometer and transfer detector during the calibration process. Transfer detector will produce the photo-generated current inside the transfer detector would be recorded as voltage V through the amplification of an amplifier. The laser radiation behind the Brewster window with regard to the optical path, recorded as P_h, could be measured directly through cryogenic radiometer. Based on the measuring principle of the cryogenic radiometer, when the characteristics of transfer detector are taken into consideration, the absolute spectral responsivity of the transfer detector can be calculated via[13]

$$R = U \cdot p \cdot N_L \cdot C \cdot \frac{V}{P_L}, \qquad (2)$$

where R is the detector responsivity, U stands for the uniform factor for the response of the detector, p represents the polarization factors of the detector, N_L stands for the linearity, C for the stability of the detector, and the output voltage of the transfer detector and the power of the incident laser are recorded as V and P_L, respectively.

The calibration result for the transfer detector consists of detector responsivity and the corresponding uncertainty of calibration process. The latter is mainly caused by the uncertainty of the measurement of laser power P_L

(Category A), the uncertainty aspects due to the characteristics of the detector (Category A), and the uncertainty because of the measurement environment, instrument, and operation conditions (Category B). Reduction on any of the previously mentioned considerations would have a positive influence on the calibration accuracy. We discovered from the actual calibration process and the materials by the other scientists[14–16] that during the measuring process of Brewster window on laser power, repeated dismounting, the transmittance and internal loss measurement error of the reconstructed calibration state would bring serious uncertainty, which therefore influenced the accuracy of laser power measurement. Table 1 shows the analysis results.

It can be known from Table 1 that during the laser power measurement process, the uncertainty caused by the repeated dismounting of the Brewster window, occupies more than 85% of the total measurement uncertainty. Aiming at reducing the negative influence caused by Brewster window during the calibration process, we first designed and accomplished the optimization schema of the calibration structure of the cryogenic radiometer in China.

We put forward a novel calibration structure based on the cryogenic radiometer, as shown in Fig. 3. The detector cavity and the cryogenic radiometer were assembled in a Y-type configuration in this calibration schema. The transfer detector, installed inside the detector cavity, could slide with cryogenic radiometer along the arc-shaped orbit. The cryogenic radiometer and the transfer detector could be switched into the optical path at different times when the calibration was carried out so as to make it available that the two pieces of equipment would be exposed to the incident beam alternately.

This novel calibration system showed in Fig. 3 mainly consists of five aspects, i.e., the cryogenic radiometer system, Y-type optical path, a detector cavity, motion control units, and a vacuum unit.

The cryogenic radiometer system, which serves the core of the whole calibration structure, was applied to measure the power of the incident laser with the accuracy being better than 1×10^{-4}. The cryogenic radiometer is of the electrical substitution characteristic and refrigerated

Table 1. Uncertainty on Measuring the Laser Power of Cryogenic Radiometer[a]

Sources	Wavelength (nm)						
	488	514	633	676	786	830	944
Electrical power	0.31	0.362	0.389	0.296	0.260	0.174	0.140
Window transmittance	1.525	0.609	1.529	0.437	0.453	0.521	0.520
Receiver absorptance				0.1			
Heating nonequivalence				0.087			
Total uncertainty	1.541	0.652	1.548	0.488	0.539	0.565	0.555
Percent	98.96	93.40	98.77	89.55	84.04	92.21	93.69

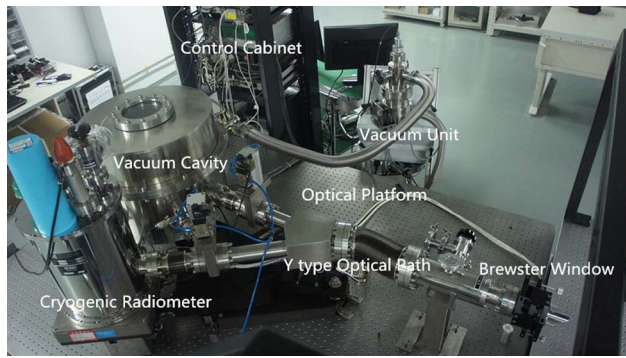[a]As per Ref. [10]. Values are multiples of 10^{-4}.

Fig. 3. Novel structure on the calibration of cryogenic radiometer.

through liquid helium. The detailed parameters of the cryogenic radiometer are listed in Table 2.

In our calibration process, the optical schema was designed in Y-type configuration. In the incident direction, evacuating valve, vacuum gauge, bellows, vacuum pipe, triangle valve, and vacuum gate valve were assembled. The evacuating valve linked the vacuum units. The vacuum of the calibration system was monitored by the vacuum gauge. Under the premise of guarantying the vacuum pumping speed, KF25 connectors were adopted for universality.

To cushion the vibration of the triangle valve, a bellows was installed which was helpful to maintain the vacuum condition. The internal and external diameters of the bellows were 80 and 108 mm. The Brewster window was placed in front of the vacuum pipe.

The diameter of the detector cavity was 500 mm and the height was 400 mm. At the bottom of the detector cavity, a CF50 flange was installed which was used to switch to the main optical path. Besides the CF50 flange, a KF25 valve and a 55 core socket were set to exhaust. There was a transparent observation window that was intercalated to monitor the inside state.

Table 2. Technique Parameter of Cryogenic Radiometer at the Anhui Institute of Optics and Fine Mechanics

Technical Specifications	
Instrument model	Cryorad II
Spectrum	0.25–50 μm
Receiver response	$2\,\mathrm{K\,mW^{-1}}$
Dynamic range	Max to 0.25 mW
Absolute accuracy	±0.005%
Receiver absorptance	>0.99998 (632.8 nm)
Refrigeration mode	Liquid nitrogen
	Liquid helium
Calibration structure	Y-type
Demount Brewster window	No

The inner translation was sealed by magnetic fluid sealing techniques to meet the need of our calibration. The migration of the inner translation was more than 150 mm. The transfer detector to be calibrated was assembled on the guide rail, which was motivated by a magnetic fluid motor to switch into the optical path (Fig. 4).

The cryogenic radiometer and the detector cavity were fixed on the motion control unit, and then the two pieces of equipment could be switched into the optical path alternately. The cryogenic radiometer could be ascended or descended therefore to make sure the equipment features accurate position alignment. Three lock carriers were installed inside the detector bin on the guide rail to accomplish the switch.

Vacuum units were for imparting a vacuum to the system and providing high-vacuum environment for the cryogenic radiometer. Vacuum units consisted of dry vacuum pump and molecular pump. The rate of dry vacuum pump reached to 4 and 200 L/S for the molecular pump. A vacuum monitor system was configured to monitor the calibration units with the range reached 1×10^5 to 1×10^{-7} Pa.

The gate valve in the cryogenic radiometer branch was locked when the whole system was put under vacuum. First, we used dry vacuum pump to impart a vacuum to the Y-type optical path and the detector cavity before the molecular pump continued the vacuum mission. The connector between the bellows and detector cavity was KF25.

With respect to the cryogenic radiometer, a special vacuum unit was applied to achieve the vacuum degree needed. When the vacuum degree in both cryogenic radiometer and detector cavity reached 1×10^{-4} Pa, the gate valve in the cryogenic radiometer branch was thus unlocked to maintain the vacuum environment.

In the novel calibration structure, the entrance pupil of the cryogenic radiometer and the transfer detector could be switched to the same position of the concentric arcs alternately and then achieved the laser power of calibration beam entering into the cryogenic radiometer and transfer detector sharing the same characteristics. Meanwhile, in the front end of the transfer detector, an aperture cylinder
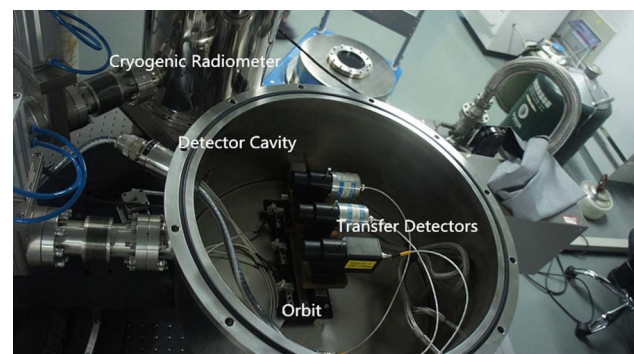

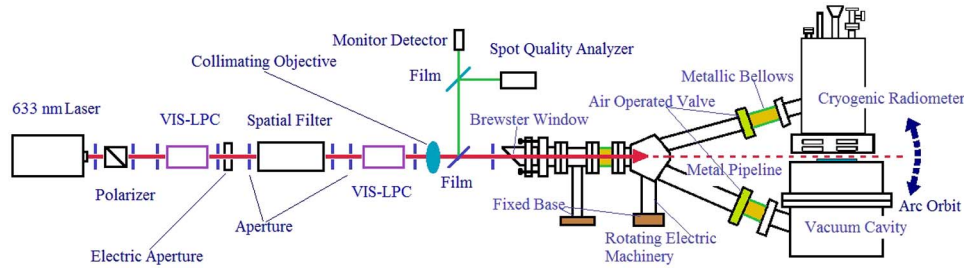Fig. 4. Transfer detector installed in detector cavity.

Fig. 5. Optical path on the calibration of cryogenic radiometer.

whose inner diameter was 6 mm was installed. The inner diameter of the aperture was same to the reception cavity of the cryogenic radiometer so that the influence of stray light on both the pieces of equipment was also identical. At last, the laser power into the cryogenic radiometer and the transfer detector could be shown as

$$P'_L = \frac{NP_h}{A}. \tag{3}$$

Therefore, it is only required to measure nonequivalence factor N of the cryogenic radiometer when the incident laser power is measured. Term A is given by National Institute of Standards and Technology (NIST) calibration report and P_h is the output value of the cryogenic radiometer.

In this novel calibration schema, we used a laser as the source to calibrate the standard transfer detector. The schema is shown as Fig. 5. The output of the laser was a linearly polarized beam; p-polarized light would thus be generated through polarizer. A laser power controller (LPC) was applied to preliminarily stabilize the input laser power. Spatial filter, which is made up of two objectives, pinhole, and aperture, was set to filter out the high-order mode and stray light which was mingled with the laser beam so that purely fundamental laser beam could be obtained. Monitor detector was for monitoring the stability of the source during the calibration process.

To verify the calibration accuracy of our new calibration schema, a comparison was made between this novel and traditional results. The details are listed in Table 3. We employ consistence factor (K) to character the distinction, which is shown as

$$K = \frac{R_{\max} - R_{\min}}{(R_{\max} + R_{\min})/2}, \tag{4}$$

where K represents the consistence of the two calibration results, and $R_{\max}$ and $R_{\min}$, respectively, stand for the maximum and minimum value of the responsivity obtained. Therefore, we got the K value, which equaled 0.4%.

From Eq. (3), we can confirm that the uncertainty of the laser power lies in the following three aspects, which are the uncertainty of the heating of equivalent current (u_N), the uncertainty of the cavity absorption (u_A), and

Table 3. Comparison on Responsivity of Transfer Detector in Novel Calibration Structure and Traditional Calibration Structure

	Absolute Spectral Responsivity (A/W)	
Detector	Traditional[a] (2008)	Novel (2014)
Trap-B	0.5069	0.5045
K	0.4%	

[a]Data given by the calibration report in 2008.

the uncertainty of the power of electricity heater (u_{Ph}). Similarly, we obtained the combined measurement uncertainty and the absolute power of the laser through the following

$$u_{P'_L}^2 = \left(\frac{P_h}{A}\right)^2 u_N^2 + \left(\frac{NP_h}{A^2}\right)^2 u_A^2 + \left(\frac{N}{A}\right)^2 u_{P_h}^2. \tag{5}$$

The relative uncertainty was calculated by

$$u_{rP'_L} = u_{P'_L}/P'_L = \sqrt{\frac{1}{N^2} u_N^2 + \frac{1}{A^2} u_A^2 + \frac{1}{P_h^2} u_{Ph}^2}$$

$$= \sqrt{u_{rN}^2 + u_{rA}^2 + u_{rP_h}^2}. \tag{6}$$

The combined uncertainty could be expressed as[17]

$$u^2(R) = \left(\frac{\partial R}{\partial U}\right)^2 u^2(U) + \left(\frac{\partial R}{\partial P}\right)^2 u^2(P) + \left(\frac{\partial R}{\partial N}\right)^2 u^2(N)$$
$$+ \left(\frac{\partial R}{\partial C}\right)^2 u^2(C) + \left(\frac{\partial R}{\partial V}\right)^2 u^2(V) + \left(\frac{\partial R}{\partial P'_L}\right)^2 u^2(P'_L),$$

$$\frac{u^2(R)}{R^2} = \frac{u^2(U)}{U^2} + \frac{u^2(P)}{P^2} + \frac{u^2(N)}{N^2} + \frac{u^2(C)}{C^2} + \frac{u^2(V)}{V^2} + \frac{u^2(P'_L)}{P'_L},$$

$$u_r(R) = \sqrt{u_r^2(U) + u_r^2(P) + u_r^2(N) + u_r^2(C) + u_r^2(V) + u_r^2(P'_L)}. \tag{7}$$

The uncertainty caused by the stray light, temperature drift, and data collection error is included in $u_r^2(V)$. The attributions of different factors on uncertainty of the transfer detector calibration results are listed and the

Table 4. Compare of Combine Uncertainty of Transfer Detector between Traditional and Novel[a]

Source	Traditional Calibration Structure (2008)[b]	Novel Calibration Optical Path (2014)
Electrical power	0.389	0.671
Window transmittance	1.529	—
Receiver absorptance	0.1	0.1
Heating nonequivalence	0.087	0.05195
Laser power total uncertainty	1.5832	0.6804
Linearity	0.434	
Spatial uniformity	1.99	
Polarization sensitivity	0.492	
Stability	0.687	
Output V	0.025	0.0244
Total uncertainty ($k = 1$)	2.715	2.321

[a]Values are multiples of 10^{-4}.
[b]Data provided by Li Shuang in 2008[13].

combined uncertainties of the two calibration approaches are compared in Table 4.

It is proved from Table 4 that our new calibration schema shows an uncertainty performance 6.804×10^{-5}, which decreased by a factor of 2 compared with the traditional result (1.5832×10^{-4}). While the measurement uncertainty of the transfer detector in novel calibration structure shows 15% less than the traditional calibration. The novel calibration structure can avoid the dismounting of Brewster window, which can greatly improve the efficiency and reduce the appearance of uncertainty.

In conclusion, we design and accomplish the optimization and upgrading on the calibration structure of cryogenic radiometer in China. We also make comparative analysis on the absolute spectral responsivity of the same transfer detector obtained from the calibration based on two different structures. The result shows that the consistence of the two calibration processes for the absolute spectral responsivity of the transfer detector is 0.4%. After the construction reform, the uncertainty decreases by 15% compared with that of the former construction. The experiment result shows that the novel calibration structure of cryogenic radiometer can reduce the uncertainty on traceability standard of radiometric calibration, avoid the dismounting of Brewster window after the calibration, improve the calibration accuracy, and eliminate the uncertainty caused by dismounting the window; therefore, it has a great significance on the calibration of transfer detector. This requires a transfer detector under tested are calibrated in a vacuum state, with vacuum compatibility requirements. If transfer detector is needed to work in the conditions of liquid nitrogen or helium refrigeration, the calibration method will no longer be suitable.

References
1. J. E. Martin, N. P. Fox, and P. G. Key, Metrologia **21**, 147 (1985).
2. P. V. Foukal, H. Kochling, and P. Miller, Appl. Opt. **29**, 988 (1990).
3. T. R. Gentile, J. M. Houston, and J. E. Hardis, Appl. Opt. **35**, 1056 (1996).
4. M. Sildoja, F. Manoocheri, M. Merimaa, E. Ikonen, I. Muller, L. Werner, J. Gran, T. Kubarsepp, M. Smid, and M. L. Rastello, Metrologia **50**, 385 (2013).
5. I. Muller, U. Johannsen, U. Linke, L. Socaciu-Siebert, M. Smid, G. Porrovecchio, M. Sildoja, F. Manoocheri, E. Ikonen, J. Gran, T. Kubarsepp, G. Brida, and L. Werner, Metrologia **50**, 395 (2013).
6. G. P. Eppeldauer, H. W. Yoon, J. Zeng, and T. C. Larason, Metrologia **49**, 112 (2012).
7. A. Fehlmannl, G. Kopp, W. Schmutz, and R. Winkler, Metrologia **49**, 34 (2012).
8. S. Cui, Z. Wang, and S. Yang, Chin. Opt. Lett. **12**, 110101 (2014).
9. J. Zhang, Y. Lin, J. Shao, and Q. Fan, Acta Metrologica Sin. **19**, 194 (1998).
10. X. Zheng, H. Wu, J. Zhang, Y. Liu, W. Zhou, L. Wang, and Y. Qiao, Chin. Sci. Bull. **45**, 1341 (2000).
11. M. Xia, J. Li, Z. Li, D. Gao, W. Pang, D. Li, and X. Zheng, Chin. Opt. Lett. **12**, 121201 (2014).
12. J. Li, X. Shi, X. Zheng, K. Chen, H. Wang, W. Zhang, and P. Xie, Scientia Sin. Phys, Mech. Astron. **41**, 749 (2011).
13. S. Li, "The Continuous Spectral Radiometric Calibration at a Wide Spectrum Based on Cryogenic Radiometer," PhD. Thesis (Anhui Institute of Optics and Fine Mechanics (CAS), 2006).
14. X. Zheng, H. Wu, J. Zhang, W. Zhou, Y. Liu, L. Wang, and Y. Qiao, Acta Opt. Sin. **21**, 749 (2001).
15. J. Li, X. Zheng, Y. Lu, W. Zhang, P. Xie, and P. Zou, Chin. Phys. Soc. **58**, 6273 (2009).
16. Z. Yang, W. Fang, Y. Luo, and Z. Xia, Chin. Opt. Lett. **12**, 101202 (2014).
17. B. N. Taylor and C. E. Kuyatt, "Guidelines for Evaluating and Expressing the Uncertainty of NIST Measurement Results," NIST technical note, 1297, available at http://www.nist.gov/pml/pubs/tn1297/index.cfm.